

Energy and magnetisation transport in non-equilibrium macrospin systems

Simone Borlenghi,^{1,2} Stefano Iubini,³ Stefano Lepri,^{4,5} Jonathan Chico,¹ Lars Bergqvist,² Anna Delin,^{2,1} and Jonas Fransson¹

¹*Department of Physics and Astronomy, Uppsala University, Box 516, SE-75120 Uppsala, Sweden.*

²*Department of Materials and Nanophysics, School of Information and Communication Technology, Electrum 229, Royal Institute of Technology, SE-16440 Kista, Sweden.*

³*Centre de Biophysique Moléculaire (CBM), CNRS-UPR 4301 Rue Charles Sadron, F-45071 Orléans, France*

⁴*Consiglio Nazionale delle Ricerche, Istituto dei Sistemi Complessi, Via Madonna del Piano 10 I-50019 Sesto Fiorentino, Italy.*

⁵*Istituto Nazionale di Fisica Nucleare, Sezione di Firenze, via G. Sansone 1, I-50019 Sesto Fiorentino, Italy*

(Dated: November 19, 2021)

We investigate numerically the magnetisation dynamics of an array of nano-disks interacting through the magneto-dipolar coupling. In the presence of a temperature gradient, the chain reaches a non-equilibrium steady state where energy and magnetisation currents propagate. This effect can be described as the flow of energy and particle currents in an off-equilibrium discrete nonlinear Schrödinger (DNLS) equation. This model makes transparent the transport properties of the system and allows for a precise definition of temperature and chemical potential for a precessing spin. The present study proposes a novel setup for the spin-Seebeck effect, and shows that its qualitative features can be captured by a general oscillator-chain model

PACS numbers: 05.60.-k, 05.70.Ln, 44.10.+i

I. INTRODUCTION

Off-equilibrium dynamics of classical and quantum many-particle systems is a wide topic, ranging from the theoretical foundations to the development of innovative ideas for nanoscale thermal management. The nanoscale control of heat flows offer promising opportunities for novel energy harvesting devices, and constitutes a fertile terrain to with possible future applications to nanotechnologies and effective energetic resources.

In this context, simple models of classical nonlinear oscillators have been investigated to gain a deeper understanding of heat transfer processes far from thermal equilibrium [1–3]. In the case of systems admitting two (or more) conserved quantities, coupled transport (for instance of energy and mass) is an issue of basic relevance in connection with thermoelectric phenomena [4] whereby temperature gradients can be employed to generate electric currents.

A related topic concerns coupled transport in magnetic systems. The recent discovery of the spin-Seebeck effect has opened the new field of spin-caloritronics [5–7], where the transport properties of thermally driven spin systems is in focus. The propagation of spin wave (SW) current driven by a thermal gradient has been extensively studied in systems of exchange coupled spins, using the well established micromagnetic formalism [8–11]. In the context of statistical mechanics, although several studies of heat transport in classical Heisenberg spin chains exists [12, 13], this topic has not been treated in detail up to now.

Here, we investigate transport in a novel setup, which consists of an array of magnetic nano-disks coupled through the magneto-dipolar interaction, and interacting with different external reservoirs. As a result, energy and magnetisation currents are carried by damped dipolar spin waves.

To obtain a better insight, we follow a simplified physical picture: one can think of a spin system as a chain of nonlinear oscillators. Intuitively, a thermal bath acts as a random

force on some part of the chain, whose effect is the propagation of oscillations (spin waves) in the system, in the form of energy and magnetisation currents. More specifically, we will model the system as an open discrete nonlinear Schrödinger (DNLS) system that steadily exchanges energy with external reservoirs, a setup that has been considered only recently [14–16]. In particular, we will employ a Langevin thermostatting scheme whereby complex white noises and dissipative couplings are added to the equation [17, 18]. Altogether, this guarantees that the chain reaches thermal equilibrium when put in contact with thermostats at the same temperature. As we will show, this approach has several advantages in terms of simplicity of description and it makes transparent the transport/thermodynamical properties of the micromagnetic system.

This paper is organised as follows. In Section II we review the equation of motion of the magnetisation for a macrospin interacting with a reservoir. In Section III we outline the derivation of the simplified oscillator model and describe its relations with the micromagnetic equations. In Section IV we study the steady-state properties of a spin-chain made of ten disks coupled via dipolar interaction through micromagnetic simulations. Using the formalism of the DNLS equation, the currents and the effective spin temperature of the system are calculated. The results are compared with the direct simulation of the oscillator model in Section V. Finally, the conclusions of this work are contained in the last Section.

II. PHYSICAL SYSTEM

The system studied here, shown in Fig. 1 consists of an array of $N = 10$ identical nano-disks made of Permalloy (Py), coupled through the dipolar interaction. The first and last disks are coupled to Langevin thermal baths with temperatures respectively T_{\pm} . Thermal fluctuations excite the SW modes of the system. In the presence of a temperature difference

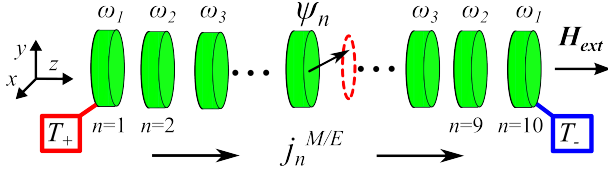


Figure 1: Chain of disks coupled via dipolar interaction. Each disk behaves as a macrospin with precession frequency ω_n . The first and last element of each chain are coupled to thermal reservoirs with temperatures T_{\pm} , that control the propagation of energy and magnetisation currents.

$\Delta T = T_+ - T_-$, the disk chain reaches a non-equilibrium stationary state where two coupled currents, of energy and magnetisation, flow from the hot (T_+) to the cold (T_-) reservoirs.

The dynamics is investigated by means of micromagnetic simulations. The cornerstone of micromagnetism is the Landau-Lifschitz-Gilbert (LLG) equation of motion for a ferromagnet [19–21]

$$\dot{\mathbf{M}} = \gamma \mathbf{M} \times \mathbf{H}_{\text{eff}} + \frac{\alpha}{M_s} \mathbf{M} \times \dot{\mathbf{M}}, \quad (1)$$

which describes the precession of the local magnetisation vector $\mathbf{M}(\mathbf{r}, t)$ around the effective field \mathbf{H}_{eff} . The first term of Eq.(1), proportional to the gyromagnetic ratio γ , accounts for the precession. The second term describes energy dissipation at a rate proportional to the dimensionless Gilbert damping parameter α . In the absence of an external driving field, such as thermal fluctuations, spin transfer torque or rf fields, the magnetisation eventually aligns with \mathbf{H}_{eff} [21, 22]. The saturation magnetisation M_s is the norm of the magnetisation vector, which depends on the material and the geometry of the sample. The thermodynamical properties of the system are described by the Gibbs free energy

$$\mathcal{F} = \mu_0 \int_V [A \Delta \mathbf{M}(\mathbf{r}, t) - \mathbf{M}(\mathbf{r}, t) \cdot \mathbf{H}_{\text{ext}} - \frac{1}{2} \mathbf{M}(\mathbf{r}, t) \cdot \mathbf{H}_{\text{dip}}] d^3 r, \quad (2)$$

μ_0 being the vacuum magnetic permeability. In the present case, Eq.(2) contains contributions respectively from exchange energy, Zeeman interaction and dipolar interactions. The effective field in Eq.(1) is given by the functional derivative $\mathbf{H}_{\text{eff}} = -(1/\mu_0) \delta \mathcal{F} / \delta \mathbf{M}$ of the Gibbs free energy with respect to the magnetisation. It is the sum of the following three terms:

$$\mathbf{H}_{\text{exc}} = -A \nabla^2 \mathbf{M}(\mathbf{r}, t), \quad (3a)$$

$$\mathbf{H}_{\text{ext}} = H \hat{z}, \quad (3b)$$

$$\mathbf{H}_{\text{dip}} = -\frac{1}{4\pi} \int_V \frac{\rho_M(\mathbf{r} - \mathbf{r}')}{|\mathbf{r} - \mathbf{r}'|^3} d^3 r' + \frac{1}{4\pi} \int_S \frac{\sigma_M(\mathbf{r} - \mathbf{r}')}{|\mathbf{r} - \mathbf{r}'|^3} d^2 r'. \quad (3c)$$

Eqs. (3a) and (3b) are respectively the exchange field with exchange constant A and the external field with intensity H

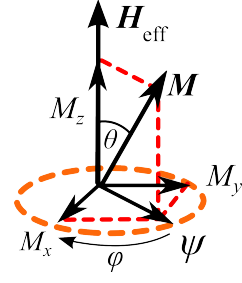


Figure 2: Macrospin \mathbf{M} precessing around the effective field \mathbf{H}_{eff} , described in terms of the stereographic projection ψ . The phase ϕ describes the dynamics in the x - y plane, while the SW power $p = |\dot{\psi}|^2$ is related to the polar angle θ (see text).

along \hat{z} . The exchange field is the short range interaction responsible for the coherent precession of the magnetisation inside each disk, while the applied field defines the precession axis. The dipolar stray field Eq.(3c) contains contributions from the volume charges $\rho_M = \nabla \cdot \mathbf{M}(\mathbf{r}', t)$ and the surface charges $\sigma_M = \mathbf{M}(\mathbf{r}', t) \cdot \hat{\mathbf{n}}$, where $\hat{\mathbf{n}}$ denotes the normal to the surface of the sample at point \mathbf{r}' . The dipolar field acts as a demagnetising field in each disk and adds a coupling between the disks. It is responsible for the nonlinearity of the LLG equation, Eq. (1).

Thermal fluctuations are introduced by adding to the effective field the stochastic term

$$\mathbf{H}_{\text{th}}(\mathbf{r}, t) = \sqrt{DT}(\eta_x, \eta_y, \eta_z), \quad (4)$$

where $\eta_j(\mathbf{r}, t)$, $j = (x, y, z)$, is a Gaussian random process with zero average and correlation $\langle \eta_j(\mathbf{r}, t) \eta_{j'}(\mathbf{r}', t') \rangle = \delta_{jj'} \delta(\mathbf{r} - \mathbf{r}') \delta(t - t')$. [23, 24]. The term $T = T(\mathbf{r})$ denotes the local temperature of the underlying phonon bath, while the coupling strength with the bath is

$$D = \frac{2\alpha k_B}{\gamma \mu_0 V_M M_s}. \quad (5)$$

Here k_B is the Boltzmann constant and V_M is the volume associated to the magnetic moment $\mathbf{M}(\mathbf{r})$.

In our micromagnetics simulations, where the sample is represented by a finite element tetrahedral mesh, the LLG equation, Eq. (1), is solved numerically at each mesh node. The coordinate \mathbf{r} is discretised and corresponds to the positions of the nodes, while V_M corresponds the volume of each mesh elements.

III. COUPLED OSCILLATOR MODEL

The dynamics of the chain is conveniently described by the volume-averaged magnetisation inside the n th disk:

$$\dot{\mathbf{M}}^n(t) = \frac{1}{V_n} \int_{V_n} \dot{\mathbf{M}}(\mathbf{r}_n, t) d^3 r_n. \quad (6)$$

Due to the uniform precession of the magnetisation in each disk, the system can be modeled as an assembly of coupled macrospins $\mathbf{M}_n(t)$. With this approximation, Eq.(1) can be written in the form of an equation of motion for an ensemble of coupled nonlinear oscillators [22]

$$i\dot{\psi}_n = \omega_n(p_n)\psi_n - i\Gamma_n(p_n)\psi_n + \sum_{n'} J_{nn'}\psi_{n'} + \sqrt{D_n(p_n)T_n}\xi_n, \quad (7)$$

where the complex SW amplitudes are defined by

$$\psi_n = \frac{M_x^n - iM_y^n}{\sqrt{2M_s(M_s + M_z^n)}}. \quad (8)$$

By writing Eq.(8) as $\psi_n = \sqrt{p_n(t)}e^{i\phi_n(t)}$, one can see that ϕ_n describes the precession of \mathbf{M} in the x - y plane, while $p_n = |\psi_n|^2$ (referred to as the local SW power) is related to the polar angle through $\theta_n = \arccos(1 - p_n)$, see Fig.2.

The first two terms on the right hand side of Eq.(7) are respectively the nonlinear frequencies $\omega_n(p_n)$ and damping rates $\Gamma_n(p_n)$ of the n th disk. Both are proportional to the effective field $\gamma|\mathbf{H}_{\text{eff}}^n \cdot \hat{z}|$ acting on each disk.

For the small precession amplitudes considered here, nonlinear effects are taken into account perturbatively by expanding into powers of p_n the frequencies and damping rates, respectively as [22] $\omega_n(p_n) \approx \omega_n + \nu p_n$, $\Gamma_n(p_n) \approx \alpha\omega_n(1 + Qp_n)$. Here ω_n , ν and Q are the coefficients of the expansion of $\omega_n(p_n)$ and $\Gamma_n(p_n)$ to the first order in p_n . The third term on the right hand side is the interlayer coupling $J_{nn'}$. In general it is a complex quantity, and its phase is related to energy gain or dissipation [18]. In the following we will consider the simple case of a uniform nearest-neighbour interaction that amounts to retain only terms containing $\psi_{n\pm 1}$ in Eq.(7) and set $J_{nn'} = J\delta_{n,n\pm 1}$. Note also that the imaginary part of $J_{nn'}$ and Γ_n are related since they both stem from the dissipative term proportional to α in the LLG equation, Eq. (1). Both the nonlinearity and the coupling are due to the dipolar field Eq.(3c). The parameters ($\omega_n, \nu, Q, J_{nn'}$) can be calculated analytically only in some simple cases, but in general they must be inferred from micromagnetic simulations [22, 25].

We consider the case where the temperature is uniform within each disk. In this case, the last term of Eq.(7) describes thermal fluctuations in terms of the *complex* Gaussian random variables $\xi_n = (\eta_x^n + i\eta_y^n)$ and the nonlinear diffusion constant $D_n(p_n)$. In the linear regime, the latter equals γD , where D is the quantity defined in Eq.(5). In the nonlinear regime $D_n(p_n)$ depends on $\Gamma_n(p_n)$, $\omega_n(p_n)$ and $J_{nn'}$ and must be fixed consistently to satisfy the fluctuation-dissipation theorem. For the single oscillator this amounts to fix $D_n(p_n) \propto \Gamma_n(p_n)/\omega_n(p_n)$ [22]. This is necessary to ensure that, for $T_n \equiv T$, the systems approaches a global canonical equilibrium at temperature T . Consistently with the small-amplitude limit, we assume $\Gamma_n(p_n) = \alpha\omega_n(p_n)$. As a consequence, the noise term in Eq.(7) becomes purely additive and $D_n(p_n)$ reduces to a constant $D = \alpha$ in units with $k_B = 1$.

Taking into account the above approximations, we simplify Eq.(7) into

$$i\dot{\psi}_n = (1 + i\alpha) \left[-\nu|\psi_n|^2\psi_n - \omega_n\psi_n - J(\psi_{n+1} + \psi_{n-1}) \right] + \sqrt{\alpha T_n}\xi_n(t). \quad (9)$$

Upon defining the ‘‘Hamiltonian’’

$$\mathcal{H} = \sum_n [\omega_n|\psi_n|^2 + \frac{\nu}{2}|\psi_n|^4 + J(\psi_n^*\psi_{n+1} + \psi_n\psi_{n+1}^*)], \quad (10)$$

where $(\psi_n, i\psi_n^*)$ are canonically conjugate variables satisfying the Hamilton equations $\dot{\psi}_n = -\partial\mathcal{H}/\partial i\psi_n^*$, Eq.(9) can be written more concisely in the form of a Langevin equation with uniform bath coupling α

$$i\dot{\psi}_n = -(1 + i\alpha) \frac{\partial\mathcal{H}}{\partial\psi_n^*} + \sqrt{\alpha T_n}\xi_n.$$

In the absence of coupling with the external baths ($\alpha = 0$), Eq.(9) is the well-known DNLS equation [26] which, at variance with its continuum limit, is not integrable [27]. Such equation describes a large class of conservative oscillating systems. Some examples include transport in biomolecules, Bose-Einstein condensates in optical lattices, mechanical oscillators and photonics waveguides [28, 29]. The dependence of ω_n on the lattice sites introduces an heterogeneity that is also connected with the nonlinear version of the Anderson tight-binding model [14, 30, 31].

In the non dissipative limit, the model admits a further constant of motion besides energy, namely, the total SW power $\mathcal{P} = \sum_n p_n$. As a consequence, the thermodynamic equilibrium phase-diagram is two-dimensional, and each equilibrium state is determined by the energy density \mathcal{H}/N and the SW density \mathcal{P}/N [32].

In the nonequilibrium regime, the local fluxes of the conserved quantities are of special interest. By computing the time derivatives of the SW power p_n and of the local energy \mathcal{H}_n , one obtains the two continuity equations [17, 18, 22, 33, 34]

$$\dot{p}_n = \mathcal{J}_n^M + j_{n+1}^M - j_n^M, \quad (11a)$$

$$\dot{\mathcal{H}}_n = \mathcal{J}_n^E + j_{n+1}^E - j_n^E, \quad (11b)$$

where

$$j_n^M = 2J \text{Im}[\psi_n^*(\psi_{n+1} - \psi_n)], \quad (12a)$$

$$j_n^E = 2J \text{Re} \left[\frac{\partial\mathcal{H}}{\partial i\psi_n} (\psi_{n+1} - \psi_n) \right]. \quad (12b)$$

are the magnetisation and energy currents associated with the hamiltonian coupling between neighboring oscillators. The remaining terms \mathcal{J}_n^M and \mathcal{J}_n^E account for the exchange with the reservoirs due to both fluctuations and damping. Their steady-state averages are computed using stochastic calculus, by evaluating the change of p_n and \mathcal{H}_n up to second order in the noise term [1]. As a result, one gets

$$\langle \mathcal{J}_n^M \rangle = 2\alpha T_n - 2\alpha \langle [\omega_n(p_n)p_n + J \text{Re}(\psi_n^*(\psi_{n+1} + \psi_{n-1}))] \rangle \quad (13)$$

A similar (but more involved) expression holds for the energy fluxes. As a preliminary test, we verified that for a generic nonequilibrium stationary state the above definitions of fluxes satisfy the local flux balance expressed in Eqs. (11a) and (11b).

For a system which is driven out-of-equilibrium from its boundaries, the local temperature represents a useful observable for the characterisation of the stationary state. Note in particular that the quantity T_n that appears in Eq.(7) specifies the temperature of the phonon bath, which in general *does not* correspond to the temperature of the system [15]. The definition of temperature for a system of interacting magnetic moments is not straightforward, since the model Hamiltonian is non separable, and one cannot relate temperature to the average kinetic energy. Within the DNLS formalism, one can use the general microcanonical definition of temperature for non separable Hamiltonians with two conserved quantities [35]. The general expression is nonlocal and rather involved, we refer to Refs.[15, 17, 35] for details. Since we are interested in the limit of low temperatures and low amplitudes, we can follow the derivation in Ref. [17] and introduce a simple approximation of the microcanonical temperature based on a mapping of the DNLS equation to a chain of nonlinear coupled rotators (XY model). Accordingly, the temperature is approximated by

$$T_{XY} = f(\langle p_n \rangle) \left[\langle \dot{\phi}_n^2 \rangle - \langle \phi_n \rangle^2 \right], \quad (14)$$

and it acquires a simple interpretation of the phase-fluctuations of the oscillator ψ_n . The function $f(\langle p_n \rangle)$ is a rescaling factor that depends on the average local power $\langle p_n \rangle$. One can also show that for $\langle p_n \rangle \ll 1$, $f(\langle p_n \rangle) = 2 \langle p_n \rangle$.

IV. MICROMAGNETIC SIMULATIONS

The micromagnetic simulations were performed with the Nmag software [36], using a tetrahedral finite element mesh with maximum size of 3 nm, of the order of the Py exchange length, and an integration time step is 1 ps. The mesh was automatically generated by the Netgen package [37].

Each disk of the chain has thickness $t = 3$ nm, radius $R = 20$ nm, and an interlayer distance $d = 3$ nm. The applied field $\mathbf{H}_{\text{ext}} = 1\text{T}$ defines the precession axis of the magnetisation along \hat{z} . The exchange stiffness $A = 1 \times 10^{-11}$ J/m corresponds to that of Py, while the other micromagnetic parameters are $M_s = 0.94 \text{ T}/\mu_0$, $\alpha = 8 \times 10^{-3}$ and $\gamma = 1.873 \times 10^{11} \text{ rad} \times \text{s}^{-1} \times \text{T}^{-1}$.

The output of the simulations consists of the ensemble of the magnetisation vectors $\{\mathbf{M}^n(\mathbf{r}_n, t)\}$, $n = 1, \dots, 10$. Each vector depends on the spacial coordinate \mathbf{r}_n inside the n_{th} disk, and the collective magnetisation dynamics of each disk is given by the volume average Eq.(6) [22, 34]

To have a basis for comparison, we consider first dynamics at zero temperature. Starting with the magnetization uniformly tilted 5 with respect to the z axis, the time evolution is computed for 30 ns. The SW power spectrum, shown in

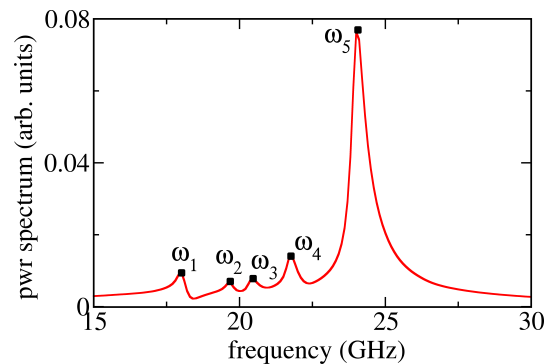


Figure 3: SW spectrum of the system at zero temperature, characterised by 5 dipolar modes.

Fig.3, is given by the absolute value of the Fourier transform of the collective variable $\Psi(t) = \sum_{n=1}^{10} \psi_n(t)$. The spectrum consists of five dipolar modes with frequencies ($\omega_1, \dots, \omega_5$) of respectively (18, 19.7, 20.5, 21.8, 24) GHz. By inspecting the spectra of the individual disks, one can see that the mode ω_1 corresponds to the precession of the first and tenth disks, the mode ω_2 to the second and ninth disks and so on until the fifth disk which precesses with frequency ω_5 , see Fig.(1). This indicates that the system has a mirror symmetry around its center, due to the fact that each disk behaves as a magnetic dipole. Aligning those dipoles in a chain gives a structure where the intensity of the dipolar field, which controls the frequencies, is symmetric around the center of the chain.

Let us now discuss the off equilibrium dynamics. We consider the configuration normally adopted to study heat transfer in chains of nonlinear oscillators [1], where the thermal baths act only at the boundaries of the system. This setup is different from the usual micromagnetic studies of the spin-Seebeck effect [8–11], where each spin is coupled to a thermal reservoir with a different temperature. The main advantage of our choice consists in that it allows to observe the spontaneous thermalisation of the system, by probing the XY temperature defined in Eq.(14), for the spins that *are not directly connected* to the thermal baths. Experimentally, this could be realised by separating the disks with thermal insulating spacers, so that energy flows are carried only by the dipolar coupling.

The simulations at finite temperature were performed starting with the magnetisation aligned along \hat{z} and evolving the system in the presence of the thermal baths for 110 ns. The relevant observables were computed after an interval of 70 ns, necessary for the system to reach the nonequilibrium steady state. The results were time averaged over the last 40 ns and then ensemble averaged over 32 samples with different realisation of the thermal noise.

The high temperature bath T_+ ranges between 5 and 30 K, while the lower temperature bath T_- is kept fix at 5 K, so that $\Delta T = T_+ - T_-$ is comprised between 0 and 25 K. The local currents are always expressed per unit coupling and are thus pure numbers. According to our convention, $j_n^{M/E}$ refers to the current propagating from disk n to disk $n + 1$ and positive (resp. negative) currents propagate from left to right (resp.

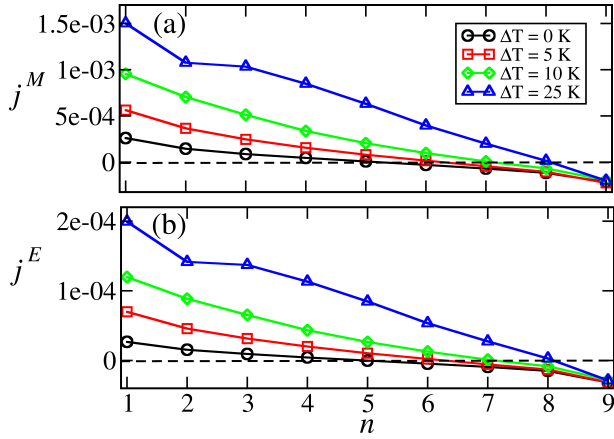


Figure 4: Profiles of magnetisation (a) and energy (b) currents computed for different values of ΔT . The profiles are symmetric for $\Delta T = 0$, and then become strongly asymmetric. The lines are guide to the eye.

from right to left).

In contrast to previous studies of the off-equilibrium DNLS, here the dissipation is both at the edges and in the bulk of the system. As a consequence, the currents do not have a flat profile in the bulk, but decrease exponentially along the chain. In the thermodynamic limit, this system is thus an insulator.

Figs.4 (a) and (b) show respectively the profiles of magnetisation and energy currents, for different values of ΔT . The two currents have similar profiles, and they do not vanish when $\Delta T = 0$ (black dots). In both cases, they are symmetric with respect to the zero-current axis. This behaviour is due to the fact that the currents generated by the two baths travel in opposite directions and decrease because of the damping, vanishing in the middle of the chain. Note that, although the local currents do not vanish at equilibrium, the total current is zero.

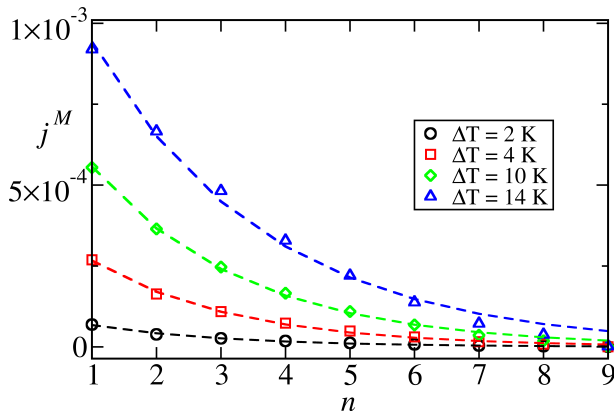


Figure 5: Profiles of the magnetisation currents for $T_- = 0$ K and different values of T_+ . The right-going current decreases exponentially along the chain. The dashed lines are fit with Ae^{-x/x_0} , for different values of the parameters (A, x_0). The energy currents have similar profiles (not reported).

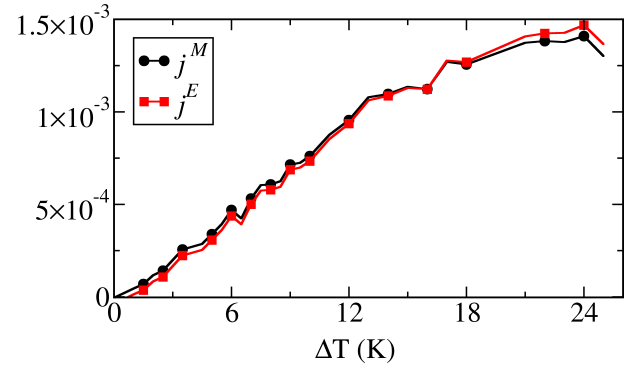


Figure 6: Currents $j^{M/E} = j_1^{M/E} + j_9^{M/E}$ injected from the reservoirs vs the temperature difference ΔT . The currents grow linearly with ΔT in the low temperature regime, and then reach a plateau. The lines are guides to the eye.

Increasing T_+ leads to the increase of the right-going currents, and moves the point where the local currents vanish.

In all these cases, the system behaves essentially as sink: the currents injected from the baths are dissipated in the bulk, so that there is no net transport. A situation where transport occurs can be observed in Fig.(5), which shows the case where $T_- = 0$ and (the right-going) current is injected only by T_+ . The current decreases exponentially, and for high enough value of ΔT remains positive until the end of the system. Note that in the thermodynamic limit this system is an insulator, due to the damping in the bulk.

Note that the local currents do not grow indefinitely with ΔT , but they saturates around $\Delta T \approx 20$ K. This can be seen more clearly in Fig.6, where the currents injected from the reservoirs $j^{M/E} = j_1^{M/E} + j_9^{M/E}$ grow linearly with ΔT until they reach a plateau for $\Delta T \approx 20$ K.

This phenomenon originates from the fact that the LLG equation is nonlinear, and consequently the frequency spectrum of the system is temperature dependent. Fig. 7 shows

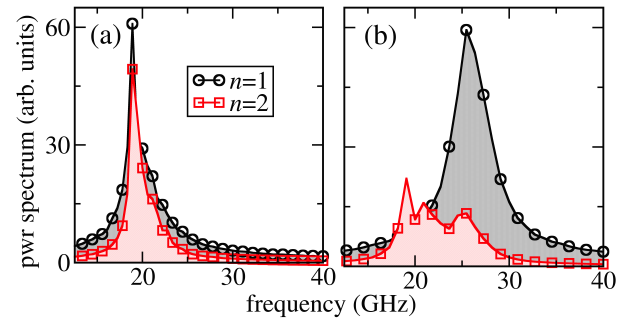


Figure 7: Finite temperature power spectra of disks 1 and 2. (a) At low temperatures ($T_{\pm} = 5$ K) regime the peaks overlap and the currents are proportional to ΔT . (b) At high temperature ($T_+ = 30$ K) the spectrum of disk 1 shifts towards high frequency, reducing its overlap with disk 2. In this condition, the current does not increase anymore with ΔT .

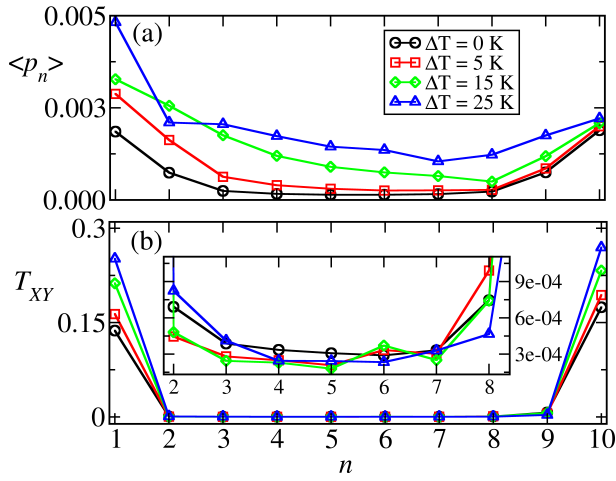


Figure 8: (a) Profiles of SW powers p_n for different values of ΔT . (b) Profiles of spin temperature T_{XY} for different values of ΔT . The inset displays a magnification of the profiles between the disks 2 and 8, which show the spontaneous thermalisation of the chain. The lines are guide to the eye.

the power spectra of the disks 1 and 2. Panel (a) displays the low temperature regime, with $T_+ = T_- = 5$ K. Thermal fluctuations excite all the modes of the system, and both disks display a broad peak between 17 and 25 GHz. The current increases linearly with ΔT as far those peaks overlap. Panels (b) show the high temperature case, where disk 1, directly connected to the hot bath, increases its frequency and does not overlap with disk 2. This situation is a manifestation of stochastic phase synchronisation (that is, the control of synchronisation through temperature) in the propagation of heat current. A similar mechanism is at the basis of spin and thermal rectifiers [33, 34, 38–40].

The profile of the local SW powers p_n is displayed in Fig. 8 (a). The powers reach the maximum at the edges, directly connected to the baths, and decay along the chain. As expected, their profile is symmetric for $\Delta T = 0$, and becomes strongly asymmetric when the temperature difference is finite. Note that the powers increase with with temperature until $\Delta T \approx 15$ K and then remain roughly constant. In this high temperature regime, p_1 keeps increasing because of thermal fluctuations, but p_2 decreases. This is due to the fact that energy remains confined in the first disk due to the de-synchronization, as previously discussed.

Fig. 8(b) shows the spin temperature profiles T_{XY} of the chain, computed for different values of ΔT . The temperature is higher at the boundaries, where phase fluctuations are given by the direct contact with the baths, and then decreases dramatically towards the center of the chain, as can be seen from the inset.

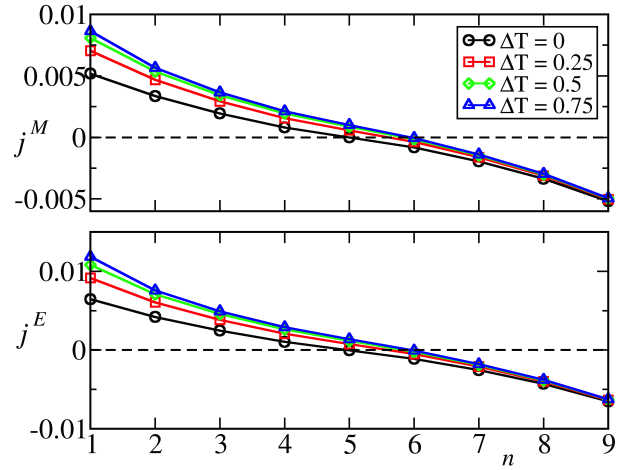


Figure 9: Simulation of Eq. (9) with $J = 0.1$, $\alpha = 0.008$, $\nu = 1$, $(\omega_1, \omega_2, \omega_3, \omega_4, \omega_5) = (1, 1.09, 1.15, 1.21, 1.33)$ and different applied temperature differences ΔT . The temperature of the leftmost reservoir spaces in the interval $T_+ = [0.5, 1.25]$, while the rightmost one is kept fixed at $T_- = 0.5$.

V. COMPARISON WITH THE OSCILLATOR MODEL

The micromagnetic simulations indicate that the system has some form of mirror symmetry around its center. Thus we model this by choosing the linear frequencies in model (9) such that $\omega_n^0 = \omega_{N-n}^0$. A relatively small coupling $J = 0.1$ has been employed. As in Section IV, the fluctuating forces are applied only at the boundaries of the system, i.e. we choose $T_n = [T_+ \delta_{n,1} + T_- \delta_{n,N}]$;

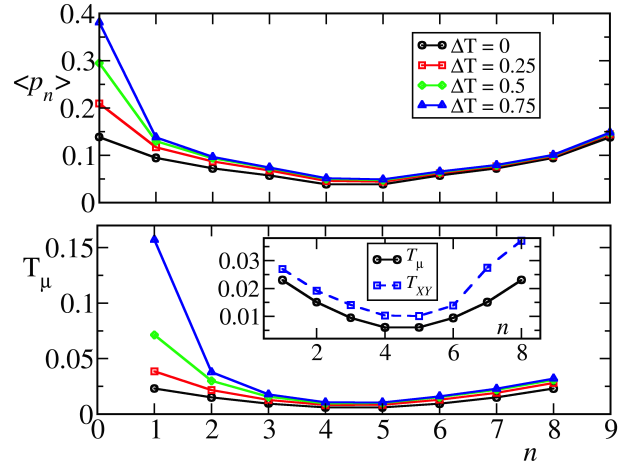


Figure 10: Simulation of Eq. (9), SW profiles and microcanonical temperature T_μ for different applied temperature differences ΔT . The parameters of the simulation are the same as in Fig. 9. For each lattice site n , the local temperature T_μ is calculated by evaluating the general definition [15, 17] on a triplet of sites centered around n . The inset of the lower panel shows a comparison between T_μ and T_{XY} for the profile with $\Delta T = 0$.

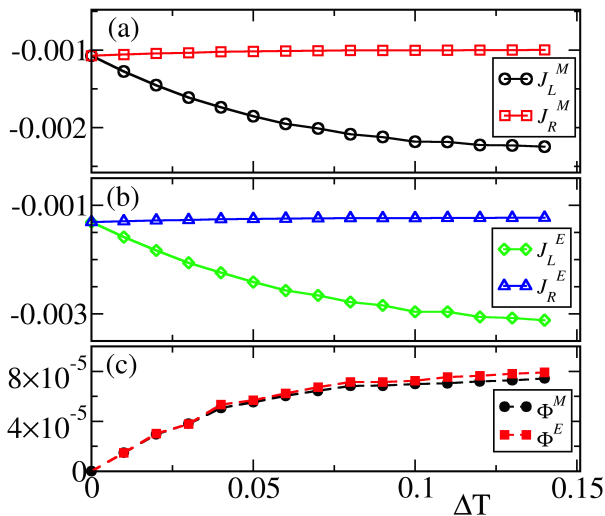


Figure 11: Simulation of Eq. (9) Boundary magnetisation (a) and energy (b) currents toward the two left and right reservoirs versus the temperature difference ΔT for $T_- = 0.05$, other parameters given in the text. Panel (c) shows the corresponding excess fluxes calculated with Eq.(15).

As a test for stationarity we evaluated the average currents from the heat baths $\sum_n \langle \mathcal{J}_n^M \rangle$ and $\sum_n \langle \mathcal{J}_n^H \rangle$ are indeed vanishing within statistical accuracy.

In Figs. 9 and 10 we show the current and SW power profiles along the chain. Comparing with the corresponding figures 4(a,b) and 8(a), the qualitative agreement is good. The lower panel of Fig. 10 reports the temperature profiles T_μ calculated with the exact microcanonical expression defined in Refs.[15, 17]. Such profiles are in good agreement with the phase temperature T_{XY} (see the inset) and qualitatively reproduce the temperature profiles calculated within the micromagnetic framework in Fig. 2. Altogether, this confirms that definition (14) is a sensible approximation in the present setup.

Finally, in panels (a) and (b) of Fig.11 we show the stationary boundary fluxes \mathcal{J}_n^M and \mathcal{J}_n^E . Nicely, they reproduce the saturation effect observed in Fig.4 with the micromagnetic simulations. It should be noted that the currents do not vanish for $\Delta T = 0$: this is simply because the system is off-equilibrium also in this case due to the presence of the dissipation in the bulk of the chain. For the very same reason, the two currents flowing at the boundary are not equal. In order to single out the purely transport contribution from the dissipative one in the boundary fluxes, we define an *excess* boundary flux $\Phi^{M,E}$ as

$$\Phi^{M,E} = \mathcal{J}_R^{M,E}(\Delta T) - \mathcal{J}_R^{M,E}(0) \quad , \quad (15)$$

that takes into account the amount of magnetisation/energy which is transported per unit time with respect to the purely dissipative symmetric profile at $\Delta T = 0$. The behaviour of $\Phi^{M,E}(\Delta T)$ is shown in Fig.11(c). Both the excess fluxes have positive sign, meaning that there is a net transport of energy

and magnetisation from left to right. Moreover they show the same saturation effect observed in panels (a) and (b).

VI. CONCLUSIONS

In this work we have illustrated the spin-Seebeck effect in a small array of coupled magnetic nanodisks and we have related to general transport properties of out-of-equilibrium chains of nonlinear oscillators. The dynamics of the disk chain has been investigated by means of micromagnetic simulations and compared with the effective model, Eq. (9). There is indeed a good qualitative agreement between the two approaches, and a good physical insight can be achieved from the coupled oscillator model.

Another remarkable result, is that the relationship with the XY model provides a simple prescription for computing the local phase temperature in the micromagnetic simulations via Eq. (14). Such observable plays a relevant role in our setup, since it allows to quantify thermal fluctuations inside the system, i.e. for macrospins that are not directly connected to the external reservoirs. This last issue is of major importance for non-standard Hamiltonians like the DNLS one, where kinetic and potential energies are not separated. Indeed, the XY approximation allows introducing the simple kinetic expression T_{XY} for the temperature, that can safely approximate the microcanonical one T_μ . This is of practical importance, considering that the microscopic definitions of T and μ are pretty much involved for a non separable Hamiltonian, like the DNLS one.

The presence of two coupled currents is related to the existence of two thermodynamic forces [41–43] ($\Delta T, \Delta\mu$), the latter being the difference of chemical potential [15, 17]. In this work we limited to the case where $\Delta\mu = 0$. Actually, chemical potential gradients can be easily accounted for within the DNLS language, by adding terms of the form $i\alpha\mu_n\psi_n$ to Eq.9 [17]. For our system of precessing spins, this is interpreted as a torque that compensates the damping and controls the magnon relaxation time towards the reservoirs [15, 17, 34]. This can be experimentally realised trough spin transfer torque [22, 44, 45]. In this case the spin-torque induces a nonequilibrium dynamics and may lead to self-sustained oscillations, thus opening a new realm of transport phenomena. We plan to investigate those setups in the next future.

Acknowledgements

We thank Prof. Magnus Johansson for illuminating discussions. We acknowledge financial support from the Swedish Research Council (VR), Energimyndigheten (STEM), the Knut and Alice Wallenberg Foundation, the Carl Tryggers Foundation, the Swedish e-Science Research Centre (SeRC) and the Swedish Foundation for Strategic Research (SSF). S.I. acknowledges financial support from the EU-FP7 project PAPERETS (GA 323901). We gratefully acknowledge the hospitality of the Galileo Galilei Institute for Theoretical Physics,

where part of this work was performed, during the 2014 workshop *Advances in Nonequilibrium Statistical mechanics*.

-
- [1] S. Lepri, R. Livi, and A. Politi, *Phys. Rep.* **377**, 1 (2003).
- [2] G. Basile, L. Delfini, S. Lepri, R. Livi, S. Olla, and A. Politi, *Eur. Phys. J.-Special Topics* **151**, 85 (2007).
- [3] A. Dhar, *Adv. Phys.* **57**, 457 (2008).
- [4] K. Saito, G. Benenti, and G. Casati, *Chem. Phys.* **375**, 508 (2010).
- [5] K. Uchida et al., *Nature* **455**, 778 (2008).
- [6] K. Uchida et al., *Nat. Mater.* **9**, 894 (2010).
- [7] G. E. W. Bauer, E. Saitoh, and B. J. van Wees, *Nat. Mater.* **11**, 391 (2012).
- [8] J.-i. Ohe, H. Adachi, S. Takahashi, and S. Maekawa, *Phys. Rev. B* **83**, 115118 (2011).
- [9] D. Hinzke and U. Nowak, *Phys. Rev. Lett.* **107**, 027205 (2011).
- [10] U. Ritzmann, D. Hinzke, and U. Nowak, *Phys. Rev. B* **89**, 024409 (2014).
- [11] S. R. Etesami, L. Chotorlishvili, A. Sukhov, and J. Berakdar, *Phys. Rev. B* **90**, 014410 (2014).
- [12] A. Savin, G. Tsironis, and X. Zotos, *Phys. Rev. B* **72**, 140402 (2005).
- [13] D. Bagchi and P. Mohanty, *Phys. Rev. B* **86**, 214302 (2012).
- [14] D. Basko, *Annals of Physics* **326**, 1577 (2011).
- [15] S. Iubini, S. Lepri, and A. Politi, *Phys. Rev. E* **86**, 011108 (2012).
- [16] W. De Roeck and F. Huveneers, *Commun. Pure Appl. Math.* (2014).
- [17] S. Iubini, S. Lepri, R. Livi, and A. Politi, *J. Stat. Mech.* p. P08017 (2013).
- [18] S. Borlenghi, S. Iubini, S. Lepri, L. Bergqvist, A. Delin, and J. Fransson, arXiv:1411.5170 (2014).
- [19] L. D. Landau and E. M. Lifshitz, in *Collected papers* (Ed. Pergamon, 1965).
- [20] T. Gilbert, *IEEE, Transaction on Magnetics* **40**, 3443 (2004).
- [21] A. G. Gurevich and G. A. Melkov, *Magnetization Oscillation and Waves* (CRC Press, 1996).
- [22] A. Slavin and V. Tiberkevich, *IEEE Transactions on Magnetics* **45**, 1875 (2009).
- [23] E. Martinez et al., *Phys. Rev. B* **75**, 174409 (2007).
- [24] G. Grinstein and R. H. Koch, *Phys. Rev. Lett.* **90**, 207201 (2003).
- [25] V. V. Naletov et al., *Phys. Rev. B* **84**, 224423 (2011).
- [26] J. C. Eilbeck, P. S. Lomdahl, and A. C. Scott, *Physica D* **16**, 318 (1985).
- [27] B. Rumpf and A. C. Newell, *Physica D: Nonlinear Phenomena* **184**, 162 (2003).
- [28] J. C. Eilbeck and M. Johansson, in *Conference on Localization and Energy Transfer in Nonlinear Systems* (2003), p. 44.
- [29] P. G. Kevrekidis, *The Discrete Nonlinear Schrödinger Equation* (Springer Verlag, Berlin, 2009).
- [30] A. S. Pikovsky and D. L. Shepelyansky, *Phys. Rev. Lett.* **100**, 094101 (2008).
- [31] G. Kopidakis, S. Komineas, S. Flach, and S. Aubry, *Phys. Rev. Lett.* **100**, 084103 (2008).
- [32] K. Rasmussen, T. Cretegny, P. G. Kevrekidis, and N. Grønbech-Jensen, *Phys. Rev. Lett.* **84**, 3740 (2000).
- [33] S. Borlenghi, W. Wang, H. Fangohr, L. Bergqvist, and A. Delin, *Phys. Rev. Lett.* **112**, 047203 (2014).
- [34] S. Borlenghi, S. Lepri, L. Bergqvist, and A. Delin, *Phys. Rev. B* **89**, 054428 (2014).
- [35] R. Franzosi, *J. Stat. Phys.* **143**, 824 (2011).
- [36] T. Fischbacher et al., *Magnetics, IEEE Transactions on* **43**, 2896 (2007).
- [37] J. Schöberl, *Computing and Visualization in Science* **1**, 41 (1997).
- [38] B. Li, L. Wang, and G. Casati, *Phys. Rev. Lett.* **93**, 184301 (2004).
- [39] J. Ren and J.-X. Zhu, *Phys. Rev. B* **88**, 094427 (2013).
- [40] J. Ren, J. Fransson, and J.-X. Zhu, *Phys. Rev. B* **89**, 214407 (2014).
- [41] L. Onsager, *Phys. Rev.* **37**, 405 (1931).
- [42] L. Onsager, *Phys. Rev.* **38**, 2265 (1931).
- [43] N. S. M. Toda, R. Kubo, *Statistical physics* (Springer-Verlag, 1983).
- [44] J. Slonczewski, *Journal of Magnetism and Magnetic Materials* **159**, L1 (1996), ISSN 0304-8853.
- [45] L. Berger, *Phys. Rev. B* **54**, 9353 (1996).